

Theoretical investigation on the excited state intramolecular proton transfer in Me_2N substituted flavonoid by the time-dependentdensity functional theory method

Hang Yin(尹航), Ying Shi(石英)
Citation: Chin. Phys. B . 2018, 27(5): 058201. **doi:** 10.1088/1674-1056/27/5/058201

Journal homepage: http://cpb.iphy.ac.cn; http://iopscience.iop.org/cpb

What follows is a list of articles you may be interested in

Accurate double many-body expansion potential energy surface of $HS_2(A^2A')$ by scaling the external correlation

Lu-Lu Zhang(张路路), Yu-Zhi Song(宋玉志), Shou-Bao Gao(高守宝), Yuan Zhang(张媛), Qing-Tian Meng(孟庆田)
Chin. Phys. B . 2016, 25(5): 053101. **doi:** 10.1088/1674-1056/25/5/053101

Ultrafast structural dynamics studied by kilohertz time-resolved x-ray diffraction

Guo Xin, Jiang Zhou-Ya, Chen Long, Chen Li-Ming, Xin Jian-Guo, Peter M. Rentzepis, Chen Jie
Chin. Phys. B . 2015, 24(10): 108701. **doi:** 10.1088/1674-1056/24/10/108701

Time-dependent density functional theoretical studies on the photo-induced dynamics of an HCl molecule encapsulated in C_{60} under femtosecond laser pulses

Liu Dan-Dan, Zhang Hong
Chin. Phys. B . 2013, 22(10): 103103. **doi:** 10.1088/1674-1056/22/10/103103

Theoretical investigation on the excited state intramolecular proton transfer in Me_2N substituted flavonoid by the time-dependent density functional theory method*

Hang Yin(尹航)[1,2] and Ying Shi(石英)[1,†]

[1] *Institute of Atomic and Molecular Physics, Jilin University, Changchun* 130012, *China*

[2] *State Key Laboratory of Supramolecular Structure and Materials, College of Chemistry, Jilin University, Changchun* 130012, *China*

(Received 27 December 2017; revised manuscript received 23 January 2018; published online 18 April 2018)

Time-dependent density functional theory (TDDFT) method is used to investigate the details of the excited state intramolecular proton transfer (ESIPT) process and the mechanism for temperature effect on the Enol*/Keto* emission ratio for the Me_2N-substited flavonoid (MNF) compound. The geometric structures of the S_0 and S_1 states are denoted as the Enol, Enol*, and Keto*. In addition, the absorption and fluorescence peaks are also calculated. It is noted that the calculated large Stokes shift is in good agreement with the experimental result. Furthermore, our results confirm that the ESIPT process happens upon photoexcitation, which is distinctly monitored by the formation and disappearance of the characteristic peaks of infrared (IR) spectra involved in the proton transfer and in the potential energy curves. Besides, the calculations of highest occupied molecular orbital (HOMO) and lowest unoccupied molecular orbital (LUMO) reveal that the electronegativity change of proton acceptor due to the intramolecular charge redistribution in the S_1 state induces the ESIPT. Moreover, the thermodynamic calculation for the MNF shows that the Enol*/Keto* emission ratio decreasing with temperature increasing arises from the barrier lowering of ESIPT.

Keywords: time-dependent density functional theory, excited state intramolecular proton transfer, intramolecular charge transfer, transition state

PACS: 82.39.Jn, 31.15.ee, 82.20.Db, 87.15.ht **DOI:** 10.1088/1674-1056/27/5/058201

1. Introduction

Excited-state intramolecular proton transfer (ESIPT), discovered first by Weller,[1] is still the subject of experimental and theoretical investigation.[2–12] Compounds that undergo ESIPT have attracted attention due to their applications in fluorescent probes,[13–15] bioimaging,[16] light-emitting materials,[17] photostabilizers,[18] and photophysical studies.[19,20] The most common spectral features of a molecule undergoing ESIPT are interesting dual fluorescence and large Stokes shift.[21]

Recently, a number of functional organic molecules based on ESIPT which exhibit dual fluorescence have been investigated extensively.[22,23] It is well known that the molecules exhibit the ESIPT properties involving a heterocyclic ring which is formed by the intramolecular hydrogen bond between a hydroxyl group and a neighboring proton acceptor.[21,24–26] Generally, ESIPT fluorophores show dual emission bands creating normal emission from Enol* form (high energy) and ESIPT emission from Keto* form (low energy).[22,27,28] It suggests that the tautomerism produces dual fluorescence and the structural geometry of the Keto emissive excited-state is significantly displaced from that of the ground state.[17,20,29]

Attention is particularly paid to the flavonoid compounds which can serve as the probe to investigate the ESIPT process and also may reveal the relationship between ESIPT and luminescence property.[30] As an important natural pigment, flavonoids constitute a major portion of natural products present in fruits and vegetables,[31,32] and are responsible for the colors in fruits and vegetables.[33] The flavonoids can be used as chemical sensors and DNA recognition due to low toxicity and attractive properties of selective binding to proteins.[34,35] The presence of hydroxyl group and proton acceptor in the flavonoids allows the molecule to undergo the ESIPT process, which means that the Keto* state is corresponding to the ESIPT emission. Meanwhile, another notable feature in the flavonoid relating to the potential intramolecular charge transfer (ICT), i.e., the Enol* state is corresponding to the ICT emission. It should be noted that the ICT is not only coexistent with ESIPT, but also across the path of ESIPT in flavonoid.[30] Respectively, the two photo-induced processes (ICT and ESIPT) have been extensively studied, however little is known about their relative importance.

Recently, Bi *et al.* used the experimental method of changing temperature to control the relative strength ratio between ICT emission and ESIPT emission for the Me_2N-substitued flavonoid (MNF) compound.[30] They found that the Keto* form (ESIPT state) emission gradually becomes stronger and the Enol* form (ICT state) emission turns weaker

*Project supported by the National Basic Research Program of China (Grant No. 2013CB922204), the National Natural Science Foundation of China (Grant Nos. 11574115 and 11704146), and the Natural Science Foundation of Jilin Province, China (Grant No. 20150101063JC).

†Corresponding author. E-mail: shi_ying@jlu.edu.cn

© 2018 Chinese Physical Society and IOP Publishing Ltd

as the temperature rises from −80 °C to room temperature. However, the mechanism for temperature effect on the luminescence properties for MNF remains unknown. A rational sensor design is dependent on the fundamental understanding of the interaction between ICT and ESIPT under different temperatures that control the sensor performance.

In the present work, we investigate the MNF molecule theoretically, aiming at exploring the details of ESIPT process for the MNF molecule and explaining the temperature effect on the Enol*/Keto* emission ratio. Especially, the structures of MNF in S_0 state and the S_1 state are optimized through the DFT and TDDFT methods, respectively. In addition, the very important information about its absorption peak and fluorescence peaks is also obtained. The differences in IR spectrum among different states are circumstantiated. Simultaneously, the potential energy curves along the proton transfer coordinate both in the ground and in the excited state are investigated as well. Moreover, we perform the thermodynamic calculation for the MNF to discover the mechanism for temperature effect on the Enol*/Keto* emission ratio, which is helpful to improve the performance of sensor based on MNF material.

2. Computational methods

In the present work, the ground-state and electronic excited-state geometry were optimized by the DFT and TDDFT[36–43] methods respectively. The Becke's three-parameter hybrid exchange function with Lee–Yang–Parr gradient-corrected correlation (B3LYP)[44,45] functional and the triple-ζ valence quality with one set of polarization functions (TZVP)[46] basis set were used in our DFT and TDDFT calculation. Moreover, no constrains for symmetry, bonds, angles, or dihedral angles were employed in the geometry optimization calculations. As for the solvent effect, dichloromethane was used as solvent in the self-consistent reaction field (SCRF) calculations through the polarizable continuum model using the integral equation formalism variant (IEFPCM).[47–49] The electronic structure was calculated using the Gaussian 09 program suite.[50] Moreover, the further processing of data is executed using the Multiwfn 3.3.9 program suite.[51]

3. Results and discussion

3.1. Absorption and fluorescence peak

Table 1 shows the calculated absorption peak and emission peak of MNF molecule. The absorption peak is calculated by vertical excitation from S_0 state to the S_1 state, and the emission peak is calculated by emission from the S_1 state equilibrium geometry to the S_0 state non-equilibrium geometry. It is obvious that the theoretical results are in good agreement with the measured absorption and emission maxima,[30] which suggests that the method is effective and credible.

Table 1. Calculated absorption peak and emission peak of MNF molecule and experimental data.

Unit: nm	Abs.	Fluo. Enol*	Fluo. Keto*
Exp.[30]	407	495	570
Theor.	428 (Homo→Lumo)	484	557

3.2. Optimized geometric structures

To depict the mechanism for de-excitation for MNF, we optimize the geometric conformations of the Enol (S_0), Enol* (S_1), and Keto* (S_1) forms shown in Fig. 1. The optimized geometries show that the intramolecular hydrogen bonds (IMHB) of MNF are formed between O_3 and H_{22} in the Enol and Enol* form, whereas an IMHB can be formed between O_4 and H_{22} in the Keto* form. In addition, the numerical values of the key geometric parameters of different electronic states can be found in Table 2. Particularly, upon exciting to Enol* state, the spacing between O_3 and H_{22} decreases from 2.008 Å to 1.860 Å, meanwhile the bond length between O_4 and H_{22} increases from 0.978 Å to 0.993 Å. In addition, the bond angles $O_3C_9C_8$ and $C_9C_8O_4$ in Enol* form are both smaller than those in Enol form. The spacing between O_3 and O_4 becomes shorter upon exciting to Enol* form. It means that the hydrogen bonded quasi-aromatic chelating ring becomes smaller after being excited. With the decreasing of the spacing between atoms, the interaction between involved atoms should

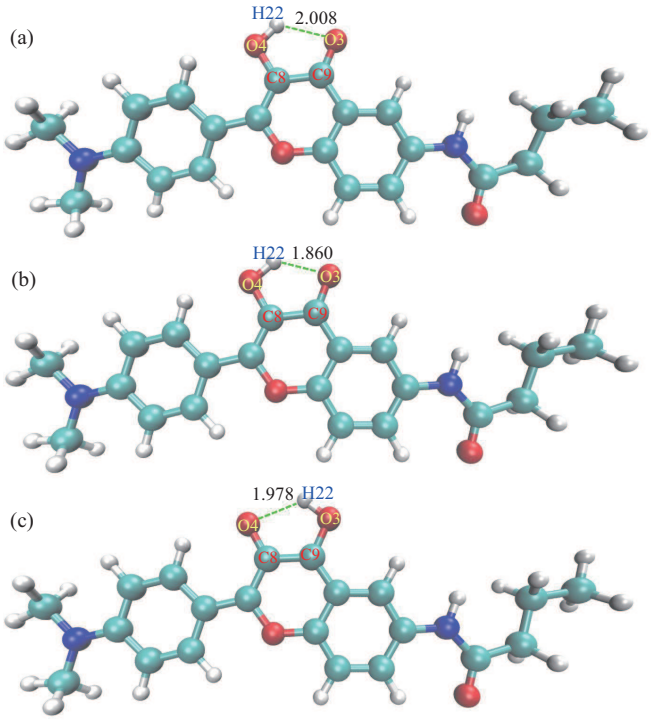


Fig. 1. (color online) Schematics of the MNF structure optimized at S_0 and S_1 states in (a) Enol, (b) Enol*, and (c) Keto* forms, showing hydrogen bond lengths, C atoms (light green), H atoms (white), O atoms (red), and N atoms (blue).

increases. It is clear that the IMHB becomes shorter and the interaction between proton O_3 and H_{22} increases, which suggests that the H_{22} has the tendency to approach O_3 which is the proton acceptor and departs from O_4 which is the proton donor. Subsequently, the MNF evolves into the Keto* form, i.e., the H_{22} transfers from O_4 to O_3. Specifically, the IMHB between O_3 and H_{22} turns into covalent bond, concomitantly the new IMHB between O_4 and H_{22} is formed. Therefore, the intramolecular hydrogen bond in the MNF molecule facilitates the ESIPT process.

Table 2. Calculated bond lengths (Å) and bond angles (deg) of the MNF molecule in different electronic states.

	C_9–C_8	C_8–O_4	C_9–O_3	O_3–O_4	O_3–H_{22}	O_4–H_{22}	$O_3C_9C_8$	$C_9C_8O_4$
Enol	1.443	1.362	1.246	2.626	2.008	0.978	119.26	114.69
Enol*	1.470	1.342	1.271	2.556	1.860	0.993	116.43	112.72
Keto*	1.445	1.275	1.342	2.603	0.983	1.978	116.12	116.44

3.3. Frontier molecular orbitals

To investigate the nature of the excited state for the MNF, the frontier molecular orbitals are analyzed. Through the absorption peak calculation, we demonstrate that the S_1 state of the MNF corresponds to the highest occupied molecular orbital (HOMO)→lowest unoccupied molecular orbital (LUMO) transition. In Fig. 2, we show schematically the frontier molecular orbital (HOMO & LUMO) for the MNF molecule. We can find that the HOMO and LUMO exhibit the π and π^* character respectively. That is to say, the S_1 state has the $\pi\pi^*$ feature which is believed to facilitate the proton transfer. It is clear that the electron density on O_3 in the LUMO increases in comparison with that in the HOMO, while that on O_4 disappears. Interestingly, the electronegativity of O_3 atom which is the proton acceptor increases a lot after being excited to the S_1 state. Meanwhile, the electronegativity of O_4 atom which is the proton donor decreases to zero upon exciting to the S_1 state. Furthermore, due to the increase of electronegativity for O_3 after being excited, the electrostatic attraction between O_3 and H_{22} increases. Conversely, the electrostatic attraction between O_4 and H_{22} decreases based on the decrease of electronegativity for O_4. That is to say, the charge distribution leads to the change of electrostatic attractions among the transferred proton, proton acceptor and proton donor, which induces the ESIPT process. Therefore, we suggest that the electronegativity change of O_3 due to the intramolecular charge redistribution in the S_1 state is not only tightly associated with changes of the acid–base properties of hydroxyl group and carbonyl group but also induces the ESIPT. In addition, it is distinct that the there is a charge transfer phenomenon between HOMO and LUMO, which demonstrates that the Enol* form is corresponding to the ICT state for the MNF molecule.

3.4. IR spectra

The other aspect relevant to the ESIPT process is the IR spectra. The vibrational frequencies of the stretching vibrations of O–H group that are involved in hydrogen bonds, as is well known, can provide a distinct signature of the ESIPT.[9] In the present work, we calculate the IR spectra (scale factor 0.9630[52]) of MNF at the S_0 and S_1 states (Enol* and Keto* forms). The calculated IR spectra of the ground state and S_1 state in a spectral range from 2800 to 3600 cm^{-1} are shown in Fig. 3, which contains not only the characteristic peaks of the O_4–H_{22} group of the S_0 and S_1 Enol forms but also the characteristic peaks of the O_4–H_{22} group of the S_1 Keto form. For S_1 tautomer form, it is a remarkable fact that the characteristic

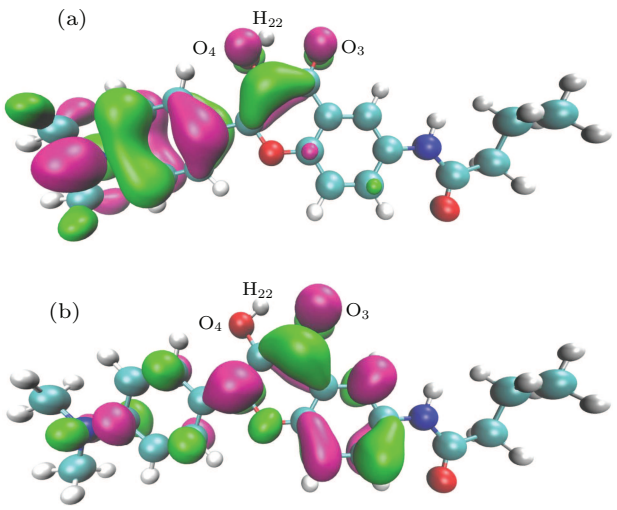


Fig. 2. (color online) Schematics of frontier molecular orbitals: (a) HOMO and (b) LUMO of MNF.

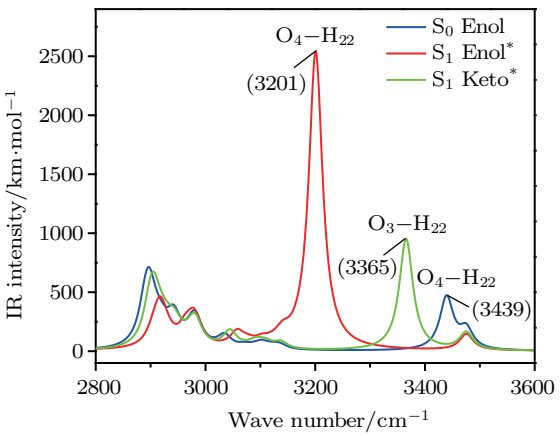


Fig. 3. (color online) Calculated IR spectra of MNF in S_0 and S_1 states (Enol form and Keto form).

peak around 3439 cm^{-1} which is assigned as ν (O_4–H_{22}) in S_0 and the characteristic peak around 3201 cm^{-1} which is assigned as ν (O_4–H_{22}) in Enol* form disappear, while the new characteristic peak around 3365 cm^{-1} which is assigned as ν (O_3–H_{22}) comes out. Thus, we can conclude that the bond of O_4–H_{22} breaks up and a new bond O_3–H_{22} forms, just as shown by the geometry optimization in Fig. 1. Consequently, the IR spectra can correlate well with the result that the H_{22} transfers from O_4 to O_3 in the S_1 state.

3.5. Potential energy curves

To demonstrate the details of the ESIPT process and explore the mechanism for de-excitation for the MNF upon excitation to the S_1 state, we calculate the potential energy curves in different electronic states. The potential energy curves are optimized by fixing the spacing between O_4 and H_{22} (proton transfer coordinate) at different values, which are recorded in Fig. 4. We can find that there are two stable geometries in S_0 state which are associated with the Enol form and Keto form respectively. It means that there is a potential possibility of ground state intramolecular proton transfer for the MNF molecule. For the S_1 state, the potential energy curve reveals that the stable points are corresponding to the coordinate 0.993 Å (Enol* form) and 1.978 Å (Keto* form), respectively. It depicts that the MNF has two stable equilibrium geometries after Frank–Condon transition to the S_1 state. To achieve the equilibrium geometry of S_1 state tautomer form, the H_{22} transfers from O_4 to O_3, which forms the new hydrogen bond between O_4 and H_{22}. Indeed, the existence of S_1 state tautomer equilibrium geometry is the direct evidence for an ESIPT process happening upon photoexcition to the S_1 state.

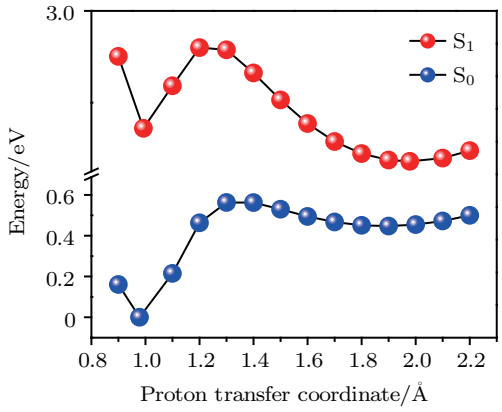


Fig. 4. (color online) Calculated potential energy curves along the proton transfer coordinate (O_4–H_{22}) of MNF in different electronic states.

3.6. Temperature effect

In the experimental investigation of Bi,[30] the fluorescence intensity ratio of F_{ICT}/F_{ESIPT} for the MNF decreases with temperature increasing (−80 °C–25°C). To find the reason why this interesting phenomenon happens, we calculate the sum of electronic and thermal free energies of transition state in the ESIPT process for the MNF at different temperatures. Figure 5 shows the variation of the transition state energy with temperature increasing from −80 to 25 °C. It is distinct that the energy is lowered from 259.7 to 258.9 kJ/mol with temperature rising, which means that the barrier of ESIPT process induced by the temperature effect becomes lower. The lower barrier promotes the ESIPT reaction, which causes greater intensity of luminescence from ESIPT state and smaller intensity of luminescence from ICT state. Therefore, we demonstrate that the barrier lowering of ESIPT process induced by temperature effect causes the ratio of F_{ICT}/F_{ESIPT} to decrease for the MNF molecule.

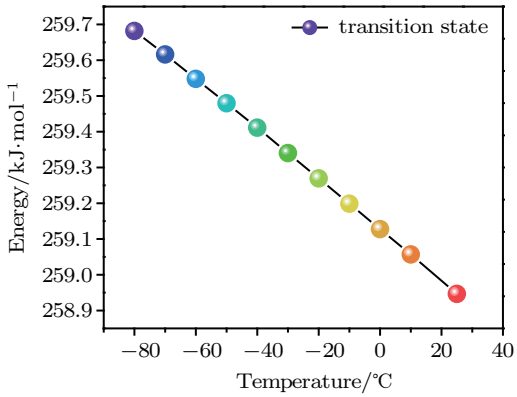


Fig. 5. (color online) Calculated sum of electronic and thermal free energies of transition state in ESIPT process for MNF at different temperatures.

4. Conclusions

The TDDFT method has been used to investigate the details of the ESIPT process and discover the mechanism for the temperature effect on the Enol*/Keto* emission ratio for the MNF. The calculation of geometric structures reveals that the interaction between O_3 and H_{22} increases upon excitation due to the shorter IMHB, and subsequently the H_{22} transfers from O_4 to O_3. The vibrational absorption spectra of the hydroxyl group in ground state and the first electronically excited-state are also calculated. The formation and disappearance of the characteristic peaks involved in the formation of hydrogen bonds in different states correlate well with the results that the H_{22} transfers from O_4 to O_3, which confirms the ESIPT process for the MNF. Through the calculation of HOMO and LUMO, we demonstrate that the electronegativity change of O_3 due to the intramolecular charge redistribution in the S_1 state induces the ESIPT. Meanwhile, the Enol* form is attributed to the ICT state. In addition, the results of calculated potential energy curves are the direct evidence for the ESIPT (Enol*→Keto*) and explain the dual fluorescence spectral feature. Furthermore, we perform the thermodynamic calculation for the MNF to discover the mechanism for temperature effect on the Enol*/Keto* emission ratio. We attribute the interesting

phenomenon to barrier lowering of ESIPT process induced by increasing temperature. It is hoped that the result is helpful in improving the performance of sensor based on MNF material.

Acknowledgment

We express heartfelt thanks to other members of our discussion group for their valuable comments.

References

[1] Weller A 1956 *Ber. Bunsenges. Phys. Chem.* **60** 1144
[2] Ma C, Yang Y, Li C and Liu Y 2015 *J. Phys. Chem. A* **119** 12686
[3] Feng Y P and Pang X F 2003 *Chin. Phys. Lett.* **20** 1662
[4] Li P L, Zheng J J and Lu Y Q 2010 *Acta Phys. Sin.* **59** 4687 (in Chinese)
[5] Yang D P, Yang G, Zhao J F, Zheng R and Wang Y S 2017 *J. Cluster Sci.* **28** 2449
[6] Yang D P, Zheng R, Wang Y S and Lv J 2017 *J. Cluster Sci.* **28** 937
[7] Amani T, Jordi M, Ali K and Kaher T 2014 *Chin. Phys. B* **23** 46101
[8] Jia X L, Li C Z, Li D L and Liu Y F 2018 *Spectrochim. Acta, Part A* **192** 168
[9] Zheng D Y, Zhang M Z and Zhao G J 2017 *Sci. Rep.* **7** 13766
[10] Han K L and Zhao G J 2011 *Hydrogen Bonding and Transfer in the Excited State* (Wiley Online Library) p. 555
[11] Zheng J J, Zhang G L, Guo Y X, Li X P and Chen W J 2007 *Chin. Phys. B* **16** 1047
[12] Wu F, Lin L, Li X P, Yu Y X, Zhang G L and Chen W J 2008 *Chin. Phys. B* **17** 1461
[13] Zhao J Z, Ji S M, Chen Y H, Guo H M and Yang P 2012 *Phys. Chem. Chem. Phys.* **14** 8803
[14] Shiraishi Y, Matsunaga Y, Hongpitakpong P and Hirai T 2013 *Chem. Commun.* **49** 3434
[15] Liu B, Wang H, Wang T S, Bao Y Y, Du F F, Tian J, Li Q B A and Bai R K 2012 *Chem. Commun.* **48** 2867
[16] Shynkar V V, Klymchenko A S, Kunzelmann C, Duportail G, Muller C D, Demchenko A P, Freyssinet J M and Mely Y 2007 *J. Am. Chem. Soc.* **129** 2187
[17] Park S, Kwon J E, Kim S H, Seo J, Chung K, Park S Y, Jang D J, Medina B M, Gierschner J and Park S Y 2009 *J. Am. Chem. Soc.* **131** 14043
[18] Paterson M J, Robb M A, Blancafort L and DeBellis A D 2005 *J. Phys. Chem. A* **109** 7527
[19] Li C Z, Ma C, Li D L and Liu Y F 2016 *J. Lumin.* **172** 29
[20] Li C Z, Yang Y G, Ma C and Liu Y F 2016 *Rsc Adv.* **6** 5134
[21] Padalkar V S and Seki S 2016 *Chem. Soc. Rev.* **45** 169
[22] Barman S, Mukhopadhyay S K, Biswas S, Nandi S, Gangopadhyay M, Dey S, Anoop A and Singh N D P 2016 *Angew. Chem. Int. Ed.* **55** 4194
[23] Alarcos N, Gutierrez M, Liras M, Sanchez F, Moreno M and Douhal A 2015 *Phys. Chem. Chem. Phys.* **17** 14569
[24] Yin H, Shi Y and Wang Y 2014 *Spectrochim. Acta Part A* **129** 280
[25] Yin H, Li H, Xia G M, Ruan C Y, Shi Y, Wang H M, Jin M X and Ding D J 2016 *Sci. Rep.* **6** 19774
[26] Liang J, Tang B Z and Liu B 2015 *Chem. Soc. Rev.* **44** 2798
[27] Tang K C, Chang M J, Lin T Y, Pan H A, Fang T C, Chen K Y, Hung W Y, Hsu Y H and Chou P T 2011 *J. Am. Chem. Soc.* **133** 17738
[28] Tang K C, Chen C L, Chuang H H, Chen J L, Chen Y J, Lin Y C, Shen J Y, Hu W P and Chou P T 2011 *J. Phys. Chem. Lett.* **2** 3063
[29] El Nahhas A, Pascher T, Leone L, Panzella L, Napolitano A and Sundstrom V 2014 *J. Phys. Chem. Lett.* **5** 2094
[30] Bi X, Liu B, McDonald L and Pang Y 2017 *J. Phys. Chem. B* **121** 4981
[31] Harnly J M, Doherty R F, Beecher G R, Holden J M, Haytowitz D B, Bhagwat S and Gebhardt S 2006 *J. Agric. Food. Chem.* **54** 9966
[32] Verma A K and Pratap R 2012 *Tetrahcdron* **68** 8523
[33] Merken H M and Beecher G R 2000 *J. Agric. Food. Chem.* **48** 577
[34] Ercelen S, Klymchenko A S, Mély Y and Demchenko A P 2005 *Int. J. Biol. Macromol.* **35** 231
[35] Xiao J B, Kai G Y, Yang F, Liu C X, Xu X C and Yamamoto K 2011 *Mol. Nutr. Food. Res.* **55** S86
[36] Yang D P, Yang Y G and Liu Y F 2014 *Spectrochim. Acta Part A* **117** 379
[37] Song P, Li Y Z, Ma F C, Pullerits T and Sun M T 2013 *J. Phys. Chem. C* **117** 15879
[38] Yang Y F, Zhao J F and Li Y Q 2016 *Sci. Rep.* **6** 32152
[39] Zhao G J and Han K L 2007 *J. Phys. Chem. A* **111** 2469
[40] Li Y Z, Qi D W, Song P and Ma F C 2015 *Materials* **8** 42
[41] Xu B B, Li Y Z, Song P, Ma F C and Sun M T 2017 *Sci. Rep.* **7** 45688
[42] Zhao G J and Han K L 2008 *J. Comput. Chem.* **29** 2010
[43] Zhao G J and Han K L 2012 *Acc. Chem. Res.* **45** 404
[44] Furche F and Ahlrichs R 2002 *J. Chem. Phys.* **117** 7433
[45] Treutler O and Ahlrichs R 1995 *J. Chem. Phys.* **102** 346
[46] Feller D 1996 *J. Comput. Chem.* **17** 1571
[47] Cancès E, Mennucci B and Tomasi J 1997 *J. Chem. Phys.* **107** 3032
[48] Cammi R and Tomasi J 1995 *J. Comput. Chem.* **16** 1449
[49] Mennucci B, Cancès E and Tomasi J 1997 *J. Phys. Chem. B* **101** 10506
[50] Frisch M J *et al Gaussian 09, Revision B.01* (Gaussian, Inc., Wallingford, 2009)
[51] Lu T and Chen F 2012 *J. Comput. Chem.* **33** 580
[52] Lukeš V, Aquino A and Lischka H 2005 *J. Phys. Chem. A* **109** 10232